Selective Growth of a C$_{70}$ Crystal in a Mixed Solvent System: From Cube to Tube

Jungah Kim,[†,‡] Chibeom Park,*[,†,‡] and Hee Cheul Choi*[,†,‡]

[†]Center for Artificial Low Dimensional Electronic System, Institute for Basic Science (IBS), 77 Cheongam-Ro, Pohang 790-784, Korea

[‡]Department of Chemistry, Pohang University of Science and Technology (POSTECH), Pohang 790-784, Republic of Korea

S Supporting Information

ABSTRACT: Cube- and tube-shaped C$_{70}$ crystals were obtained selectively by reprecipitation using a combination of mesitylene (good solvent) and isopropyl alcohol (poor solvent). Both crystals include mesitylene molecules in their lattices; the ratios of C$_{70}$ to mesitylene were 1:2 in C$_{70}$ cubes and 1:0.7 in C$_{70}$ tubes. The volume ratio of mesitylene to IPA is a key parameter for the selective growth of C$_{70}$ cubes and C$_{70}$ tubes, rather than the supersaturation ratio, which governs crystal morphology in many other cases. Thus, we propose that the absolute amount of mesitylene near C$_{70}$ molecules determines the crystallization pathways for forming the C$_{70}$·2(mesitylene) or C$_{70}$·0.7(mesitylene) phase, which finally result in C$_{70}$ cubes or C$_{70}$ tubes, respectively.

C$_{70}$·2(mesitylene)   C$_{70}$·0.7(mesitylene)
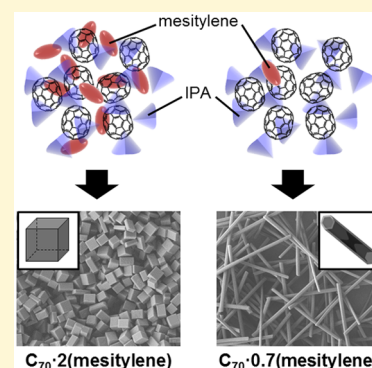
INTRODUCTION

The controllability of the morphology in molecular crystals is beneficial for studies of morphology-dependent property changes.[1−3] Crystallization of molecules that possess high-density sp^2 electrons is of special interest because the resulting crystals allow systematic investigation of the properties that commence from not only crystal facets on which molecular arrangements are dissimilar but also different crystal structures. For example, pentacene wires and disks having identical crystal structures exhibit drastic differences in optical properties because of the presence or absence of (010) plane facets.[2] Other examples are rubrene crystals and 2,5,8,11-tetra-*tert*-butylperylene crystals that show the changes in waveguiding and photoluminescence (PL) properties upon crystallization.[4,5] Hence, the development of the growth method for producing crystals in various geometries is one of the key prerequisites for such studies.

Among various methods, solution-phase crystallization is a useful method because the crystallization environment can be controlled by adjusting diverse parameters. For crystallization of fullerene molecules, solution-phase crystallization methods include drop-drying,[6−10] solvent vapor annealing,[11,12] liquid−liquid interfacial precipitation (LLIP),[13−18] and reprecipitation.[19−25] All of these methods resemble conventional recrystallization methods that exploit abrupt changes in solubility at heterointerfaces. However, one important difference for fullerene crystallization is that the good solvent molecules interact closely with fullerene molecules by hydrophobic or charge-transfer interactions to distort the most thermodynamically stable self-organization pattern of fullerene. That is, the solvent is involved directly in the crystallization of

fullerene molecules as a secondary lattice component. Since the first example of a solvent-intercalated C$_{60}$ crystal was reported,[26] efforts have been made to control the morphology of solvent-intercalated fullerene crystals and to understand the underlying crystallization mechanism. Although the solvent can affect the morphology of the fullerene crystal,[9,15,20] the correlation between the solvent and the morphology of the resulting fullerene crystals has recently been systematically evaluated. For example, the morphology of a C$_{60}$ crystal is strongly affected by the molecular shape of the solvent, as exemplified by C$_{60}$ dots, wires, and disks that are crystallized in the presence of *n*-hexane (pseudo-1D), *m*-xylene (pseudo-2D), and CCl$_4$ (pseudo-3D) solvents, respectively.[6]

In comparison to that of C$_{60}$, morphology-controlled crystallization of C$_{70}$ has been rarely reported[10,20,27] because its ellipsoidal molecular shape and the coexistence of energetically similar phases at room temperature make its crystallization difficult to control.[28,29] Nevertheless, recent reports imply that C$_{70}$ can also crystallize into a specific morphology upon solvent intercalation. For example, use of *m*-xylene or toluene produces 1D C$_{70}$ crystals such as nanowires and nanotubes,[17,20,24] and cocrystallization of C$_{70}$ with mesitylene produces high yields of cube crystals with a very narrow size distribution.[25] One common limitation in morphology control for both C$_{60}$ and C$_{70}$ crystals is that specific solvent molecules should be replaced to alter their morphologies, for example, from *m*-xylene for C$_{60}$ wires to

CCl_4 for C_{60} disks, and from *m*-xylene for C_{70} tubes to mesitylene for C_{70} cubes.[6,15,24,25] However, other options are still available if the solvent intercalation can be controlled by adjusting the crystallization environment.

We report a simple method for controlling the morphology of C_{70} crystals to be either cube or tube without replacing specific solvents, but by simply controlling the volume ratio of C_{70}-mesitylene to isopropyl alcohol (IPA). All crystals grown by this method exhibit PL stronger than that of C_{70} powder. Results of systematic experiments with various solvent combinations indicate that cocrystallization of C_{70} and solvent is affected by the volume ratio of mesitylene to IPA, but not by the supersaturation ratio.

■ EXPERIMENTAL SECTION

Growth of C_{70} Crystals. As-received C_{70} powder (MTR Ltd., 99.0%) was dissolved in mesitylene (Alfa Aesar, 98%) under ultrasonication for 3 h to prepare starting solution (C_{70}-mesitylene). A concentration-controlled C_{70}-mesitylene solution was mixed with IPA (Fisher Scientific, 99.9%) at various volume ratios and ultrasonicated for 30 s. The mixed solution was kept at room temperature for designated times. For further characterization, the precipitated crystals were transferred to Si substrate or to a Cu transmission electron microscopy (TEM) grid (Ted Pella, Inc., 400 mesh) by dropping several aliquots of final solution and drying residual solvents by blowing N_2 gas. For tube-dominant samples, the precipitated crystals were filtered and rinsed with copious amounts of IPA to prevent destruction of wires during the evaporation of residual solvents. The filtered tubes were redispersed in IPA and transferred to the appropriate substrate.

Characterization. Morphologies of C_{70} crystals were examined using a scanning electron microscope (SEM, JEOL, JSM-7401F). The crystal structure of C_{70} crystals was analyzed by powder X-ray diffraction [XRD, 5D beamline at Pohang Accelerator Laboratory (λ = 1.2390 Å)], TEM (Carl Zeiss, EM 912 omega), and selected area electron diffraction (SAED). The X-ray wavelength was scaled to Cu Kα (λ = 1.54057 Å) radiation to facilitate comparison with previous reports. The absorption spectrum for measuring the concentration of C_{70} in solutions was obtained using a UV−vis spectroscope (Agilent 8453). To confirm the presence of solvent molecules in C_{70} crystals, gas chromatography−mass spectrometry (GC−MS) was performed after redissolving crystals in chloroform (Sigma-Aldrich, contains 0.5− 1.0% ethanol as a stabilizer). The relative amount of mesitylene in the C_{70} crystal was confirmed by thermogravimetric analysis (TGA, scinco TGA N-1000) under N_2 gas by setting 800 °C as the maximal temperature with a rate of increase of 10 °C/min. PL experiments were performed using a home-built fluorescence microscope. Specifically, the optical microscope (Olympus BX51) is combined with a mercury lamp (Nikon, 130 W) and fluorescence filters (Omega Optical, λ_{ex} = 500−550 nm; Thorlabs, λ_{em} > 610 nm). The PL images were obtained using a CCD camera (Jenoptik, ProgRes C3), and PL spectra were obtained using a monochromator (DongWoo Optron Co., Ltd., DM-320i) connected to another CCD camera (Andor, iDus 420).

■ RESULTS AND DISCUSSION

When 4 mL of a C_{70}-mesitylene solution was added to 16 mL of IPA and kept for 12 h, homogeneous cube-shaped C_{70} crystals grew in high yield with average size of 3 μm in each dimension (Figure 1a). The total concentration of C_{70} in the mixed solvent was ~0.1 mM; the shape, size, and yield of the C_{70} cubes obtained under this condition agree well with those of a previous report.[25] In contrast, when the volume ratio of C_{70}-mesitylene to IPA was changed from 1:4 to 1:30 without a change in the total volume (20 mL), tube-shaped (1D) C_{70} structures were formed; they had average diameter of 800 nm
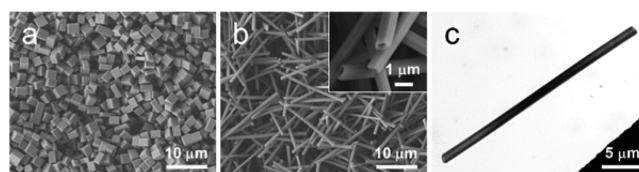

Figure 1. (a and b) SEM images of C_{70} cubes and C_{70} tubes formed at volume ratios of 1:4 and 1:30 (C_{70}-mesitylene:IPA), respectively. (c) Low-magnification TEM image of a C_{70} tube.

and an average length of 20 μm (Figure 1b). The center of the C_{70} tube was filled, whereas both ends had a hollow interior space (Figure 1c); this observation means the growth rate is faster at the edge than inside. This center-blocked tube is due to concentration depletion of C_{70} near the center of the seed, which is often observed in other organic/inorganic tube-shaped crystals,[30−32] including fullerene crystals.[20,23,33]

The crystal structure of each type of crystal was analyzed by X-ray diffraction (XRD). Although both types of crystal showed intense diffraction peaks, the XRD patterns were completely different (Figure 2a). The XRD pattern of C_{70} cubes agreed
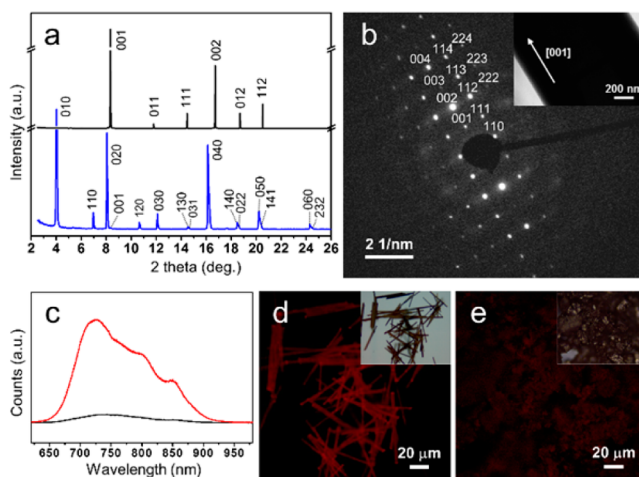

Figure 2. (a) XRD pattern of C_{70} cubes (top) and C_{70} tubes (bottom). (b) SAED pattern of C_{70} tubes and a corresponding bright field TEM image. (c) PL spectra of C_{70} tubes (red) and C_{70} powder (black). (d and e) PL images of C_{70} tubes and C_{70} powder, respectively.

well with that of a previous report (Figure 2a, top).[25] In contrast, the XRD pattern of C_{70} tubes matched no known C_{70} crystal. Therefore, we determined the crystal structure of C_{70} tubes by using the plane-spacing equation with Bragg's law.[34] As a result, the crystal structure of the C_{70} tube was indexed as a hexagonal system having lattice parameters of a = 25.36 Å and c = 10.58 Å (a/c = 2.40), which is similar to that of 1D solvated C_{60} nanocrystals (wire, rod, and whisker) except for a slightly increased lattice parameter (Figure 2a, bottom).[6,7,9,12,16,35] The SAED pattern of the C_{70} tube (Figure 2b) indicated that the tube is single-crystalline and that the growth axis is [001]; this conclusion was confirmed by a simulated SAED pattern (Figure S1 of the Supporting Information). According to the crystallographic information from our experimental results and previous reports, C_{70} molecules are more loosely packed in C_{70} tubes than in C_{70} cubes, forming linear solvent channels along the tube axis. (See schematically drawn molecular packing models for a C_{70} cube and a C_{70} tube in Figure S2 of the Supporting Information.)

Highly crystalline C_{70} crystals have enhanced PL.[10,25] Similarly, C_{70} tubes had PL higher than that of regular C_{70} powder (Figure 2c−e). The PL peak positions did not differ significantly between C_{70} tubes and cubes. This similarity indicates that the interaction the between C_{70} molecules is weaker in the crystals than in the powder; i.e., the high crystallinity grants a higher degree of long-range order to C_{70} molecules in the crystals than in the C_{70} powder. This highly ordered arrangement of C_{70} molecules in a C_{70} tube would significantly reduce the number of nonradiative pathways and thereby increase the level of radiative exciton recombination.

Although it has been reported that C_{70} crystals can be grown into 1D structures in specific solvent,[10,18,24] the work presented here is a remarkable demonstration that their morphology can be controlled from tube to cube in a single-type mixed solvent by simply varying the volume ratio of a good solvent to a poor solvent. To evaluate which solvent is more directly influencing the morphology control, we have identified the solvent cocrystallized with C_{70} by GC−MS and TGA. GC−MS analysis showed a peak at a retention time of ∼7.4 min (Figure 3a); this
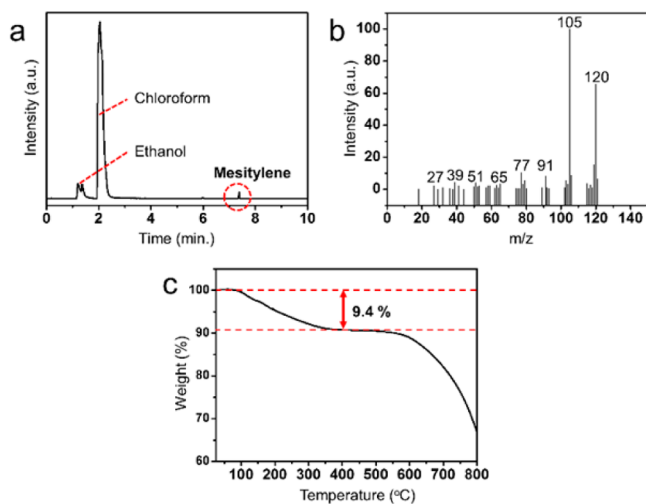
Figure 3. (a) GC data of C_{70} tubes. (b) Mass spectrum corresponding to the red circle in panel a. (c) TGA data of C_{70} tubes obtained with a rate of increase of 10 °C/min under a N_2 gas flow.

peak corresponds to mesitylene according to the MS spectrum that shows a major peak at m/z 105 (Figure 3b). Note that chloroform was a solvent used for GC−MS analysis and contained ethanol (0.5−1.0%) as a stabilizer. Therefore, mesitylene, not IPA, was incorporated into the crystals. The molar ratio of C_{70} to mesitylene in a tube was derived by TGA under N_2 (Figure 3c); the weight decreased by ∼9.4% as the temperature was increased from room temperature to 450 °C. This change indicates that the composition molar ratio of C_{70} to mesitylene is ∼1:0.7; this mesitylene content was ∼$\frac{1}{3}$ of that in C_{70} cubes (molar ratio of 1:2). This result implies that the relative amount of mesitylene is the key factor for the determination of morphology.

To evaluate the effect of the molar composition of mesitylene, control experiments were performed at a fixed total concentration of C_{70} (0.3 mg mL^{-1}) and a total solution volume of 20 mL, but at various volume ratios from 1:1 to 1:64 (C_{70}-mesitylene/IPA). The morphology of the C_{70} crystal is retained as a cube when the IPA content is increased to 1:7. However, when the relative amount of mesitylene is

significantly reduced by further increasing of the IPA content over 1:15, C_{70} is crystallized into a tube (Figure 4, top row).
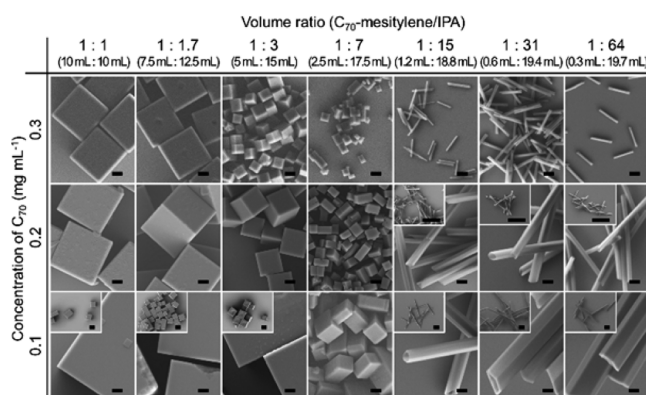
Figure 4. SEM images of C_{70} crystals at various volume ratios of C_{70}-mesitylene to IPA. The scale bar is 1 μm and in the insets 10 μm.

Similar trends were observed at C_{70} concentrations of 0.2 and 0.1 mg mL^{-1} (Figure 4, middle and bottom rows); the only notable difference is that the average size of cubes and diameter of tubes increased significantly as the C_{70} concentration decreased, probably because the decrease in C_{70} concentration reduced the number of nucleation sites.[25,36,37]

Generally, the crystallization process during reprecipitation is explained by the emulsion droplet model,[38−42] which suggests that solute and good solvent form droplets very quickly because contact between the solute molecule and poor solvent is energetically unfavorable. Subsequently, good solvent diffuses into poor solvent at a rate that depends on their miscibility. When the concentration of solute molecules in the droplet reaches the saturation point, solute molecules begin to nucleate. The nucleus formed in each droplet generates one crystal, or multiple nuclei collide to form a large crystal. In both cases, the size of the final crystal is limited by the quantity of solute molecules in each droplet, so it is proportional to the concentration of the initial solution.

However, in our case, the relationship between solute concentration and crystal size (Figure 4) was exactly the opposite of the relationship predicted by the emulsion droplet model.[38−42] Dynamic light scattering (DLS) results confirm that this reverse trend is still valid at even higher IPA ratios. When C_{70}-mesitylene solutions of various concentrations were mixed with IPA while keeping a volume ratio of 1:400, the crystal size dispersed in a mixed solution decreased as the concentration of the initial solution increased (Figure S3a of the Supporting Information, red line). In contrast, the size of C_{60} crystals obtained with a combination of toluene (good solvent) and acetonitrile (poor solvent) increased as the concentration increased when the volume ratio was kept at 1:400 (Figure S3a of the Supporting Information, black line) as well as at 1:3 (Figure S3b of the Supporting Information), as predicted by the emulsion droplet model.[38] This result implies that the crystallization of C_{70} molecules in our system does not follow the emulsion droplet model. Rather, C_{70}, mesitylene, and IPA seem to mix homogeneously as a supersaturated solution in which the number of nucleation sites is affected by the solute concentration.

When crystallization occurs under a supersaturated condition, the supersaturation ratio influences the relative growth rate of different facets and is therefore widely considered to be a

determining factor for the final morphology of organic/inorganic crystals.[4,5,37,43,44] This dependency of crystal morphology on supersaturation ratio is also observed in C_{60} crystallization.[22] To check whether our system also depends on the supersaturation ratio, we calculated supersaturation ratios for each case shown in Figure 4. For the equilibrium concentration of C_{70} (C_0) in the mixed solution, mesitylene and IPA were first mixed at volume ratios from 1:1 to 1:64, and excess C_{70} powder was dissolved by sonication followed by filtration. Then the concentrations of C_{70} were calculated using intensity values at two wavelengths (335 and 472 nm) in the UV−vis absorption spectrum (Figure 5a).[45] The equilibrium
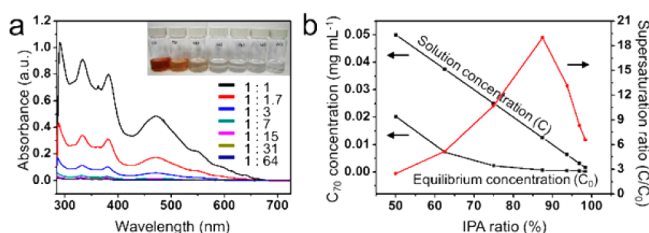

Figure 5. (a) Absorption spectra of saturated C_{70} solutions dissolved in a mesitylene/IPA mixture. The inset shows the actual colors. (b) Supersaturation ratios (C/C_0, red) depending on the volume ratio of C_{70}-mesitylene to IPA, which corresponds to the third row of Figure 4. The solution concentration (C) and equilibrium concentration (C_0) of C_{70} are shown as black lines.

concentration (C_0) decreases nonlinearly as the IPA volume ratio increases, mainly because of complex interactions of mesitylene, IPA, and C_{70} molecules. In contrast, the final concentration (C) in the mixed solution used for crystallization decreases linearly as the IPA volume ratio increases because the initial concentration of C_{70} in the solution is fixed (Figure 5b). Such different tendencies of C and C_0 lead to a nonmonotonic change in the supersaturation ratio. When the initial concentration of C_{70} was 0.1 mg mL^{-1} (third row of Figure 4), the supersaturation ratio (C/C_0) gradually increased to 87.5% of the IPA ratio, at which C_{70} cubes form (Figure 5b, red). However, C/C_0 decreased again at an IPA ratio of >87.5%, in which C_{70} tubes form. That is, both cubes and tubes can form over a similar range of C/C_0 values; therefore, the difference in morphology of C_{70} crystals is more directly related to the volume ratio of solvents than to the difference in supersaturation ratio.

Crystallization methods were compared to identify how the volume ratio of C_{70}-mesitylene to IPA affected the morphology of the C_{70} crystal. Solution-phase reactions for fullerene crystals are classified into two methods according to the crystallization environment. One includes monosolvent (good solvent) crystallization such as drop-drying,[6−10] SVA,[11,12] and evaporation,[46] in which a reduced amount of solvent changes the local solubility and the fullerene molecules start to nucleate. The other method is bisolvent crystallization such as LLIP[13−18] and reprecipitation[19−25] that uses a decrease in solubility upon addition of poor solvent. In the latter case, the good solvent environment near fullerene molecules can be efficiently controlled by changing the amount of poor solvent while the amount of good solvent molecules is sufficient throughout the crystallization process in the monosolvent crystallization method.

The importance of the mesitylene environment for the crystallization of C_{70} was confirmed by additional experiments

with different poor solvents (Figure S4 of the Supporting Information). When IPA was replaced with other alcohols (methanol, ethanol, propan-1-ol, and butan-1-ol), cube-shaped C_{70} crystals and corresponding XRD patterns were obtained at a low poor solvent ratio (1:2 volume ratio). However, at a high poor solvent ratio (1:30 volume ratio), C_{70} crystals showed anisotropic shapes and the XRD patterns deviated from those of a simple cubic structure, regardless of the type of poor solvents except methanol. This result implies formation of new phases of C_{70} containing mesitylene. However, the supersaturation ratio does not seem to be the main factor for this. For the sake of clarity, we plotted the supersaturation ratios as a function of poor solvent ratio for each case; the trends are almost similar to the case of IPA, while the values vary (Figure S5a of the Supporting Information). In spite of the same supersaturation ratio ($C/C_0 \sim 5$), C_{70} crystals obtained at a propan-1-ol ratio of 82% have cube shapes (Figure S5b of the Supporting Information), while those obtained at an ethanol ratio of 98% have anisotropic morphologies with a hexagonal cross section (Figure S5c of the Supporting Information). The most possible scenario is that the absolute amount of mesitylene near C_{70} molecules during crystallization determines the phase of C_{70} crystals because the morphologies of C_{70} crystals depend on only the volume ratio of good and poor solvents. Specifically, mesitylene-sufficient and mesitylene-deficient environments generate the cubic phase $[C_{70} \cdot 2(\text{mesitylene})]$ and hexagonal phase $[(C_{70} \cdot 0.7(\text{mesitylene})]$, respectively. One exceptional case, in which only cube-shaped crystals with a simple cubic crystal structure are formed regardless of the C_{70}-mesitylene:methanol (v/v) ratio, can be explained by other factors. Considering the high polarity and negligible C_{70} solubility of methanol, it seems that the mixing of methanol and mesitylene is not fast enough to provide a mesitylene-deficient environment. Similarly, the differences in the morphology of anisotropic crystals among different poor solvents may be ascribed to other factors such as miscibility of various alcohols and mesitylene.

The possibility that crystallization morphology can be controlled by mesitylene:IPA volume ratio in other cases was examined by performing the same experiment using C_{60}. At all volume ratios of mesitylene to IPA except 1:1, tube-shaped C_{60} crystals were obtained; at a 1:1 ratio, irregular aggregates formed (Figure S6 of the Supporting Information, top row). C_{60} molecules crystallize into 2D plates when the solvent combination consists of toluene and *tert*-butyl alcohol,[47] and to 3D shapes (popcornlike or polygons) when the solvent combination consists of toluene and ethanol,[22] but morphology-selective growth was not observed with various volume ratios of good to poor solvent (Figure S6 of the Supporting Information, middle and bottom rows). Morphology-selective growth may occur during C_{60} crystallization: irregular granules, rather than nanowires, start to form as the volume ratio of C_{60}-toluene to IPA changes from 1:1.[48] However, in our case, C_{70} crystals show a clear difference in their molar compositions and crystal structures that depends only on the volume ratio of mesitylene to IPA. Therefore, C_{70}-mesitylene is one of the unique fullerene-solvated crystal systems that possesses more than two energetically stable phases at room temperature; this diversity of stable states would allow selective growth of C_{70} crystals to either cubes or tubes, depending on the mesitylene environment.

On the basis of all of these experimental results, we propose a mechanism of selective growth of the C_{70} cube and C_{70} tube by

reprecipitation (Figure 6). After C_{70}-mesitylene and IPA had been mixed, the solution quickly becomes nearly homogeneous
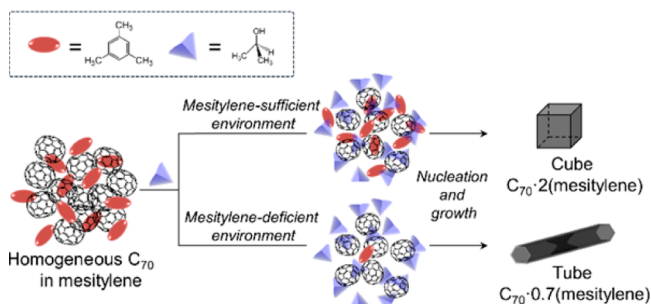

Figure 6. Schematic illustration of the growth mechanism of C_{70} cubes and C_{70} tubes. When IPA is added to a C_{70}-mesitylene solution, mesitylene and IPA form a nearly homogeneous solution because of their good miscibility. Depending on the mesitylene environment, C_{70} molecules crystallize into cubes or tubes.

because of the good miscibility of mesitylene and IPA. Almost at the same time, the concentration of C_{70} exceeds the saturation point, thereby inducing C_{70} molecules to form nuclei in quantities that are governed by the C_{70} concentration in an initial C_{70}-mesitylene solution. During the crystallization process, mesitylene molecules near C_{70} molecules are intercalated as a secondary lattice component because of chemical interactions such as van der Waals and $\pi-\pi$ interaction.[7,40] In this step, the absolute amount of mesitylene near C_{70} has a crucial effect on the crystallization, which is effectively controlled by the relative quantity of IPA. Mesitylene-sufficient and methylene-deficient environments drive C_{70} molecules to crystallize into phases that contain more mesitylene [$C_{70}\cdot2$(mesitylene)] and less mesitylene [$C_{70}\cdot0.7$(mesitylene)], which then generate cube- and tube-shaped mesitylene-solvated C_{70} crystals, respectively. Both shapes form when the C_{70}-mesitylene:IPA (v/v) ratio is between 1:9 and 1:13 (Figure S7 of the Supporting Information); therefore, the boundary of the volume ratio for formation of the C_{70} cube and C_{70} tubes is between these values.

CONCLUSION

Cube- and tube-shaped mesitylene-solvated C_{70} crystals can be grown selectively by reprecipitation in a mixture of mesitylene (good solvent) and IPA (poor solvent). The C_{70} cubes and C_{70} tubes have different crystal structures, and different mesitylene contents intercalated in the crystal. However, the morphology-selective growth is not explained by the difference in supersaturation ratio, which is widely accepted in other cases; furthermore, the crystallization process of C_{70} molecules does not follow the conventional emulsion droplet model. It is more likely that C_{70} cubes and C_{70} tubes are formed under mesitylene-sufficient and -deficient conditions, respectively; this result indicates that the mesitylene environment is the factor that determines the morphology. Thus, we newly propose a mechanism of morphology-selective growth of C_{70} crystals. In this mechanism, crystallization starts from a homogeneously mixed solution because of the good miscibility of mesitylene and IPA. Depending on the absolute amount of mesitylene near C_{70} molecules, which is determined by the mesitylene:IPA volume ratio, crystallization proceeds along two different pathways to form the $C_{70}\cdot2$(mesitylene) or $C_{70}\cdot0.7$(mesitylene) phase, which result in C_{70} cubes or C_{70} tubes,

respectively. We believe that this study provides important insight into the crystallization of fullerene molecules and provides opportunities to investigate morphology-dependent properties in various organic crystals.

ASSOCIATED CONTENT

Ⓢ Supporting Information

Simulated SAED pattern of the C_{70} tube, molecular packing models for the C_{70} cube and C_{70} tube, DLS and SEM data showing concentration-dependent size changes of fullerene crystals, XRD data and SEM images of C_{70} crystals obtained with other poor solvents, supersaturation ratio graph in the mixture of C_{70}-mesitylene and four different alcohols and SEM images of C_{70} crystals obtained at the same supersaturation ratio with different alcohols, SEM images of C_{60} crystals obtained by reprecipitation, and SEM images of C_{70} crystals grown with C_{70}-mesitylene:IPA (v/v) ratios between 1:9 and 1:13. This material is available free of charge via the Internet at http://pubs.acs.org.

AUTHOR INFORMATION

Corresponding Authors

*E-mail: choihc@postech.edu.
*E-mail: chibeom.park@gmail.com.

Notes

The authors declare no competing financial interest.

REFERENCES

(1) Park, C.; Park, J. E.; Choi, H. C. *Acc. Chem. Res.* **2014**, *47*, 2353.
(2) Park, J. E.; Son, M.; Hong, M.; Lee, G.; Choi, H. C. *Angew. Chem., Int. Ed.* **2012**, *51*, 6383.
(3) Wang, X.; Li, H.; Wu, Y.; Xu, Z.; Fu, H. *J. Am. Chem. Soc.* **2014**, *136*, 16602.
(4) Huang, L.; Liao, Q.; Shi, Q.; Fu, H.; Ma, J.; Yao, J. *J. Mater. Chem.* **2010**, *20*, 159.
(5) Zhang, X.; Zhao, C.; Lv, J.; Dong, C.; Ou, X.; Zhang, X.; Lee, S.-T. *Cryst. Growth Des.* **2011**, *11*, 3677.
(6) Park, C.; Song, H. J.; Choi, H. C. *Chem. Commun.* **2009**, 4803.
(7) Wang, L.; Liu, B.; Yu, S.; Yao, M.; Liu, D.; Hou, Y.; Cui, T.; Zou, G.; Sundqvist, B.; You, H.; et al. *Chem. Mater.* **2006**, *18*, 4190.
(8) Li, H.; Tee, B. C.-K.; Cha, J. J.; Cui, Y.; Chung, J. W.; Lee, S. Y.; Bao, Z. *J. Am. Chem. Soc.* **2012**, *134*, 2760.
(9) Wang, L.; Liu, B.; Liu, D.; Yao, M.; Hou, Y.; Yu, S.; Cui, T.; Li, D.; Zou, G.; Iwasiewicz, A.; et al. *Adv. Mater. (Weinheim, Ger.)* **2006**, *18*, 1883.
(10) Yao, M.; Fan, X.; Liu, D.; Liu, B.; Wågberg, T. *Carbon* **2012**, *50*, 209.
(11) Colle, R.; Grosso, G.; Ronzani, A.; Gazzano, M.; Palermo, V. *Carbon* **2012**, *50*, 1332.
(12) Kim, J.; Park, C.; Park, J. E.; Chu, K.; Choi, H. C. *ACS Nano* **2013**, *7*, 9122.
(13) Sathish, M.; Miyazawa, K.; Sasaki, T. *Chem. Mater.* **2007**, *19*, 2398.
(14) Larsen, C.; Barzegar, H. R.; Nitze, F.; Wågberg, T.; Edman, L. *Nanotechnology* **2012**, *23*, 344015.
(15) Sathish, M.; Miyazawa, K. *J. Am. Chem. Soc.* **2007**, *129*, 13816.
(16) Minato, J.; Miyazawa, K. *Carbon* **2005**, *43*, 2837.
(17) Miyazawa, K. *J. Am. Ceram. Soc.* **2002**, *85*, 1297.

(18) Miyazawa, K.; Minato, J.; Yoshii, T.; Suga, T. *Sci. Technol. Adv. Mater.* **2005**, *6*, 388.

(19) Chong, L. C.; Sloan, J.; Wagner, G.; Silva, S. R. P.; Curry, R. J. *J. Mater. Chem.* **2008**, *18*, 3319.

(20) Masuhara, A.; Tan, Z.; Kasai, H.; Nakanishi, H.; Oikawa, H. *Jpn. J. Appl. Phys.* **2009**, *48*, 050206.

(21) Jin, Y.; Curry, R. J.; Sloan, J.; Hatton, R. A.; Chong, L. C.; Blanchard, N.; Stolojan, V.; Kroto, H. W.; Silva, S. R. P. *J. Mater. Chem.* **2006**, *16*, 3715.

(22) Jeong, J.; Kim, W.-S.; Park, S.-I.; Yoon, T.-S.; Chung, B. H. *J. Phys. Chem. C* **2010**, *114*, 12976.

(23) Bae, E.; Kim, N. D.; Kwak, B. K.; Park, J.; Lee, J.; Kim, Y.; Choi, K.; Yi, J. *Carbon* **2010**, *48*, 3676.

(24) Liu, D.; Yao, M.; Wang, L.; Li, Q.; Cui, W.; Liu, B.; Liu, R.; Zou, B.; Cui, T.; Liu, B.; et al. *J. Phys. Chem. C* **2011**, *115*, 8918.

(25) Park, C.; Yoon, E.; Kawano, M.; Joo, T.; Choi, H. C. *Angew. Chem., Int. Ed.* **2010**, *49*, 9670.

(26) Fleming, R. M.; Kortan, A. R.; Hessen, B.; Siegrist, T.; Thiel, F. A.; Marsh, P.; Haddon, R. C.; Tycko, R.; Dabbagh, G.; Kaplan, M. L.; et al. *Phys. Rev. B* **1991**, *44*, 888.

(27) Liu, D.; Cui, W.; Yu, N.; Liu, R.; Liu, D.; Xu, Y.; Quan, C.; Liu, B.; Li, Q.; Liu, B. *CrystEngComm* **2014**, *16*, 3284.

(28) Meingast, C.; Gugenberger, F.; Roth, G.; Haluška, M.; Kuzmany, H. *Z. Phys. B: Condens. Matter* **1994**, *95*, 67.

(29) Vaughan, G. B. M.; Heiey, P. A.; Fischer, J. E.; Luzzi, D. E.; Ricketts-Foot, D. A.; McGhie, A. R.; Hui, Y.-W.; Smith, A. L.; Cox, D. E.; Romanow, W. J.; et al. *Science* **1991**, *254*, 1350.

(30) Yoon, S. M.; Hwang, I.-C.; Kim, K. S.; Choi, H. C. *Angew. Chem., Int. Ed.* **2009**, *48*, 2506.

(31) Yin, L.-W.; Bando, Y.; Golberg, D.; Li, M.-S. *Adv. Mater. (Weinheim, Ger.)* **2004**, *16*, 1833.

(32) Mayers, B.; Xia, Y. *Adv. Mater. (Weinheim, Ger.)* **2002**, *14*, 279.

(33) Ji, H.-X.; Hu, J.-S.; Tang, Q.-X.; Song, W.-G.; Wang, C.-R.; Hu, W.-P.; Wan, L.-J.; Lee, S.-T. *J. Phys. Chem. C* **2007**, *111*, 10498.

(34) Cullity, B. D. *Element of X-ray Diffraction*, 2nd ed.; Addison-Wesley Inc.: Manila, The Philippines, 1978.

(35) Ramm, M.; Luger, P.; Zobel, D.; Duczek, W.; Boeyens, J. C. A. *Cryst. Res. Technol.* **1996**, *31*, 43.

(36) Söhnel, O.; Garside, J. *Precipitation: Basic principles and industrial applications*, 1st ed.; Butterworth-Heinemann Ltd.: London, 1992.

(37) Ouyang, J.; Pei, J.; Kuang, Q.; Xie, Z.; Zheng, L. *ACS Appl. Mater. Interfaces* **2014**, *6*, 12505.

(38) Alargova, R. G.; Deguchi, S.; Tsujii, K. *J. Am. Chem. Soc.* **2001**, *123*, 10460.

(39) Ghosh, H. N.; Sapre, A. V.; Mittal, J. P. *J. Phys. Chem.* **1996**, *100*, 9439.

(40) Patnaik, A. *J. Nanosci. Nanotechnol.* **2007**, *7*, 1111.

(41) Chung, H.-R.; Kwon, E.; Oikawa, H.; Kasai, H.; Nakanishi, H. *J. Cryst. Growth* **2006**, *294*, 459.

(42) Nakanishi, H.; Katagi, H. *Supramol. Sci.* **1998**, *5*, 289.

(43) Xia, Y.; Yang, P.; Sun, Y.; Wu, Y.; Mayers, B.; Gates, B.; Yin, Y.; Kim, F.; Yan, H. *Adv. Mater. (Weinheim, Ger.)* **2003**, *15*, 353.

(44) Nichols, P. L.; Sun, M.; Ning, C. *ACS Nano* **2011**, *5*, 8730.

(45) Semenov, K. N.; Charykov, N. A.; Keskinov, V. A.; Piartman, A. K.; Blokhin, A. A.; Kopyrin, A. A. *J. Chem. Eng. Data* **2010**, *55*, 13.

(46) Agafonov, V.; Céolin, R.; André, D.; de Bruijn, J.; Gonthier-Vassal, A.; Szwarc, H.; Rodier, N.; Dugué, J.; Toscani, S.; Sizaret, P.-Y.; et al. *Chem. Phys. Lett.* **1993**, *208*, 68.

(47) Sathish, M.; Miyazawa, K.; Hill, J. P.; Ariga, K. *J. Am. Chem. Soc.* **2009**, *131*, 6372.

(48) Miyazawa, K.; Hotta, K. *J. Cryst. Growth* **2010**, *312*, 2764.